Journal of Catalysis 352 (2017) 505–514

Contents lists available at ScienceDirect

Journal of Catalysis

journal homepage: www.elsevier.com/locate/jcat

Stabilization of active, selective, and regenerable Ni-based dimerization catalysts by condensation of ethene withinordered mesopores

Iker Agirrezabal-Telleria, Enrique Iglesia *

Department of Chemical and Biomolecular Engineering, University of California at Berkeley, Berkeley, CA 94720, USA

ARTICLE INFO

Article history:
Received 15 April 2017
Revised 30 May 2017
Accepted 18 June 2017

Keywords:
Ethene dimerization
Reactivity effects of intrapore liquid phase
Transition state treatments and non-ideal thermodynamics
Active, selective and stable Ni catalyst

ABSTRACT

This study reports the high and stable ethene dimerization turnover rates conferred upon Ni-based active sites at subambient temperatures by the condensation of liquid ethene reactants within ordered mesopores in Al-MCM-41. Such active and stable catalysts do not require the activators or co-catalysts essential for organometallic Ni-based catalysts and their robust porous framework allows their full regeneration by thermal treatments in inert or oxidizing environments when deactivation occurs. Dimerization rates (per Ni) are independent of Ni content below Ni^{2+}/H^{+} exchange ratios of unity, consistent with isolated $(Ni\text{-}OH)^{+}$ cations as active moieties, and with the formation of inactive NiO oligomers at higher Ni contents. Both CO and 2,6 di-tertbutylpyridine, used as titrants of Ni centers and protons, respectively, fully suppressed reactivity, indicating that the Ni^{2+} and OH^{-} centers in $(Ni\text{-}OH)^{+}$ are involved in stabilizing the kinetically-relevant C—C formation transition state. Deactivation constants decreased abruptly to undetectable values at those temperatures and ethene pressures that formed an extended liquid phase within the MCM-41 mesopores that confine the Ni active sites. This remarkable shift from rapid to undetectable deactivation reflects how intrapore liquids preferentially stabilize the late transition states that mediate the desorption of bound 1-butenes before subsequent isomerization and C—C bond formation events during one surface sojourn. Their preferential desorption inhibits the formation of regioisomers and larger oligomers, thus inhibiting deactivation while also leading to very high C_4 selectivities among products and to the predominant presence of 1-butene among linear C_4 alkenes. Such unprecedented stability and high selectivities allow accurate kinetic measurements and their rigorous mechanistic interpretation in terms of transition state formalisms of chemical dynamics in thermodynamic non-ideal media. Dimerization turnovers involve kinetically-relevant C—C bond formation between unbound ethene molecules and an ethene bound at low coverages on $(Ni\text{-}OH)^{+}$ moieties. Such catalytic sequences lead to dimerization rates with a nearly second-order dependence in ethene fugacity, but with an effective rate constant that benefits from the stabilization of the C—C bond formation transition state as intrapore liquids form. The essential elimination of deactivation events and secondary reactions by such liquids leads to dimerization rates and 1-butene selectivities that are much higher at 240–260 K with liquid-filled mesopores than at 448 K, conditions that maintain all species in their gaseous form. In addition to their significant practical impact, these results provide compelling evidence for the ability of an extended liquid to create a thermodynamically non-ideal environment that markedly alters reaction pathways through the selective stabilization of specific transition states based on their location along the reaction coordinate for a given elementary step.

Published by Elsevier Inc.

1. Introduction

The formation of C—C bonds via alkene dimerization provides attractive routes to fuels and chemicals. Ethene, in particular, is the predominant product of thermal cracking processes, especially with natural gas condensate as the feedstock, thus making it an attractive reactant in dimerization routes to larger alkenes [1,2]. Both Cossee-Arlman [3,4] and metallacycle [2] mechanisms have been proposed as plausible dimerization pathways on homogeneous catalysts; in contrast, the precise nature of the active sites on Ni-based solid catalysts remains uncertain, as is also the case for the extent to which the mechanistic details and site requirements proposed for homogeneous catalysts can be extended to

* Corresponding author.
E-mail address: iglesia@berkeley.edu (E. Iglesia).

http://dx.doi.org/10.1016/j.jcat.2017.06.025
0021-9517/Published by Elsevier Inc.

Ni-based aluminosilicates, which do not require activators or co-catalysts [5-9]. Alkene oligomerization is also catalyzed by solid Brønsted acids (H^+); their turnover rates (per proton) depend sensitively on acid strength, because stronger acids form more stable conjugate anions at ion-pair transition states, and on the nature of inorganic frameworks that provide voids of molecular dimensions and stabilize transition states through van der Waals contacts [10]. Solid acids typically operate at higher temperatures than Ni-based homogeneous catalysts; such temperatures lead to facile hydride and methyl shifts and to skeletal isomers and regioisomers at relative concentrations predominantly dictated by thermodynamics [11].

Ni-based metal organic frameworks (MOF) [12–14] and organometallic complexes [15,16] give higher oligomerization rates (per Ni center) and 1-akene selectivities than solid Brønsted acids, but they require the use of aluminoxane activators or co-catalysts in large excess and the presence of solvents or reactants as a bulk liquid phase. These Ni-based systems also exhibit rapid deactivation and require complex regeneration protocols to avoid structural and catalytic degradation, thus limiting their use in practical large-scale oligomerization processes. Cationic Ni species dispersed on oxides (ZrO_2, TiO_2) and Ni^{2+} cations exchanged onto zeotypes [17–19] catalyze ethene oligomerization without the need for co-catalysts, but at lower rates (per Ni) than organometallic Ni complexes. NiO domains interacting with O-H groups on B_2O_3–Al_2O_3 [20] and Al-MCM-41 [21] have also been reported to catalyze alkene dimerization.

Cationic Ni species dispersed on mesoporous Al-MCM-41 [22–26] or Al-SBA15 [22] give higher rates (per Ni) than Ni cations exchanged onto FAU [27] or BEA [28] zeolites. Dimerization rates increase with Ni content on these mesoporous aluminosilicates and then reached nearly constant values [26], consistent with a number of active sites limited by the density of exchange sites on the Al-MCM-41 hosts and with such exchanged species as the sole active centers. At the temperatures required for their use as practical dimerization catalysts (>400 K), Ni-based samples deactivate rapidly and require frequent regenerations [22,24,29,30], thus precluding the unequivocal elucidation of the nature of the active Ni species, the relevant elementary steps, and the primary or secondary nature of butene regioisomers and larger oligomers [9].

Here, we report that intrapore condensation of ethene within MCM-41 leads to stable Ni reactivity and to very high turnover rates that, in fact, exceed at these subambient temperatures those previously reported on similar composition at much higher temperatures (>400 K). The resulting stability permits rigorous assessments of the mechanism and nature of the active sites. These active sites consist of $(Ni\text{-}OH)^+$ grafted onto exchange sites in Al-MCM-41, as shown by dimerization rates (per catalyst mass) that increase with Ni content up to saturation exchange stoichiometries. Dimerization rates are suppressed by CO titrants, which bind selectively to Lewis acid sites (Ni^{2+}) and by 2,6-di-*tert*-butylpyridine, which selectively titrates OH^- sites at $(Ni\text{-}OH)^+$ species, consistent with the concerted involvement of OH^- and Ni^{2+} in the $(Ni\text{-}OH)^+$ species in dimerization turnovers. The unique Ni site reactivity and stability achieved by the presence of liquid alkenes within MCM-41 mesopores allows accurate kinetic analysis of dimerization routes and the use of transition state theory formalisms appropriate for thermodynamically non-ideal systems to interpret reactivity in terms of elementary steps. Such treatments also show that Ni site stability is conferred by the preferential solvation of late desorption transition states, which prevents subsequent oligomerization and isomerization events before desorption and leads to higher 1-butene and C_4 selectivities in products at the low temperatures required for the formation of an extended liquid phase within MCM-41 mesopores.

2. Methods section

2.1. Ni-MCM-41 catalyst synthesis

Ni-MCM-41 (0.1–14.7%wt. Ni; XNi; X = Ni^{2+}/H^+) was prepared by contacting $Ni(NO_3)_2{\cdot}6H_2O$ solutions (0.05–0.5 M; 99.9%, Sigma-Aldrich) in deionized water (resistivity ~0.06 μS cm^{-1}) with Al-MCM-41 (0.01 g/cm^3, Si/Al = 40, Sigma-Aldrich) while stirring for 24 h in a round-bottomed flask placed within an oil bath at 353 K. Solids were recovered by filtration, treated in ambient air at 393 K for 12 h, and treated in flowing air (ultra dry, Praxair; 0.5 $cm^3\ g^{-1}\ s^{-1}$) by heating to 823 K at 0.083 K s^{-1} and holding for 3 h.

2.2. Ethene dimerization rates and product selectivity

Ethene dimerization rates were measured in a stainless steel tubular reactor (6.4 mm × 3 cm). Samples (10 mg; 125–180 μm aggregates) were diluted with SiO_2 (1:50 mass; Davisil-62, Sigma-Aldrich, treated in air, 1073 K, 8 h). Catalysts were treated in a flow of dry air (ultra dry, Praxair; 0.5 $cm^3\ g^{-1}\ s^{-1}$) by heating to 823 K (0.083 K s^{-1}, 0.5 h hold) and flushed with He (99.999%, Praxair) before cooling to reaction temperatures and introducing ethene (99.999%, Praxair) at 10–20 mol $g^{-1}\ h^{-1}$. Temperatures were measured with a K-type thermocouple (K-type, Omega) and controlled electronically (Watlow 982). Subambient temperatures were maintained by balancing the flow of a cold N_2 stream with resistive heating using electronic controllers. Pressure was maintained electronically (LF-1, Equilibar). Concentrations of reactant ethene and products were measured by flame ionization detection after chromatographic separation (Agilent 6890; HP-1 methyl silicone, 25 m, 0.32 mm diameter, 1.05 μm film).

2.3. Site titration methods

The number of accessible protons in the Al-MCM-41 sample (Si/Al = 40, Sigma-Aldrich) was measured by titration with 2,6-di-*tert*-butylpyridine (DTBP, >97%, Sigma-Aldrich). The Al-MCM-41 sample was treated using the same procedures used to prepare Ni-Al-MCM-41 catalysts (as described in Section 2.1), using a HNO_3 (Sigma-Aldrich, 70%, AR grade) solution of the same pH as the Ni precursor solutions (pH = 3.3–3.7). Solids were recovered by filtration and treated in flowing air as described in Section 2.1. Before titration, Al-MCM-41 (40 mg) were treated in flowing dry air (ultra dry, Praxair, 21.5% O_2, 0.4 $cm^3\ g^{-1}s^{-1}$) by increasing the temperature from ambient to 823 K at 0.083 K s^{-1} and holding for 0.5 h, then flushed with He (99.999%, Praxair) at 100 $cm^3\ min^{-1}\ g^{-1}$ and 823 K for 1 h and temperature set to 448 K. The H^+ content of this Al-MCM-41 was measured by contact with DTBP (0.5 kPa, 0.01 $mol_{DTBP}\ g^{-1}\ h^{-1}$) in flowing He. DTBP was introduced as a *n*-hexane (99%, Sigma-Aldrich) solution (1:25 DTBP/*n*-hexane molar ratio) using a syringe pump (Cole Parmer, 60061 Series). All gas flows were metered using electronic flow controllers (Porter).

DTBP titrations at 448 K were also carried out during ethene dimerization on Ni-MCM-41 samples. Before titration experiments, Ni-MCM-41 samples were treated as described above. During titration, ethene (0.1 MPa, 20 mol $g^{-1}\ h^{-1}$) was introduced together with 0.5 kPa DTBP (0.01 mol $g^{-1}\ h^{-1}$, as a solution in *n*-hexane). DTBP concentrations were measured by gas chromatography. DTBP flow was stopped after dimerization rates reached undetectable levels; no desorption of DTBP was detected in the effluent thereafter, indicative of irreversible adsorption. Titrations with CO were carried out during ethene reactions (243 K; 1.5 MPa ethene) on Ni-MCM-41 samples, containing Ni^{2+}/H^+ ratios of 0.1 and 0.8, by injection of 0.5 cm^3 pulses of 1% CO/He (ultra dry, Praxair; 1.5 MPa) at

1 h intervals with concurrent measurements of dimerization rates using the chromatographic protocols described above.

2.4. Additional characterization methods

N_2 uptakes were measured at its normal boiling point using a volumetric physisorption unit (ASAP 2020, Micromeritics). As-synthesized catalysts were first degassed at 623 K (heating rate, 10 K min^{-1}) for 4 h in vacuum. Ni contents were measured using inductively-coupled plasma atomic emission spectrometry (ICP-A ES; Galbraith Laboratories). Infrared spectra of chemisorbed CO and DTBP were collected in a Nicolet NEXUS 670 infrared spectrometer equipped with a Hg-Cd-Te (MCT) detector cooled with liquid N_2. Self-supported Ni-MCM-41 wafers (40 mg) were sealed within a quartz vacuum infrared cell fitted with NaCl windows. During CO chemisorption, samples were treated in flowing He (99.999%, Praxair) at 2.5 $cm^3\ g^{-1}\ s^{-1}$ by increasing the temperature from ambient to 823 K at 0.083 K s^{-1}, holding for 1 h at 823 K and cooled to 263 K. CO (1 kPa in He, ultra dry, Praxair; 0.5 $cm^3\ g^{-1}\ s^{-1}$) was introduced into the infrared cell and the spectra of chemisorbed CO collected with 2 cm^{-1} resolution in the 4000–400 cm^{-1} spectral range by averaging 64 scans. During DTBP chemisorption, samples were pretreated at 673 K for 1 h in flowing He, cooled to 448 K and treated in 1 kPa DTBP in He for 0.5 h. The cell was evacuated before spectra were taken at 448 K.

3. Results and discussion

3.1. Identification of active species during ethene dimerization

Dimerization rates are reported here as the combined molar rates of formation rates of C_4 and C_6 alkene chains, which account for most (>99.5%) of the products formed. These rates (per mass) at 243 K and 1.5 MPa ethene increased linearly with increasing Ni^{2+}/H^+ ratios in Ni-Al-MCM-41 up to stoichiometric ratios of unity, and then reached nearly constant rates at higher ratios (Fig. 1; H^+ from 2,6-di-*tert*-butylpyridine titration before Ni exchange). Three types of Ni species exchanged onto H^+ sites of Al-MCM-41 (Type I, II and III) and one type of bulk NiO structure (type IV) can form during contact of aqueous Ni^{2+} cations with Al-MCM-41 (Fig. 2). The low H^+ areal densities (0.1 H^+ nm^{-2}, determined from titration, Section 2.3) favor $(Ni\text{-}OH)^+$ species over isolated Ni^{2+} cations (type III, Fig. 2), because the latter require vicinal protons from Al-MCM-41 that are unlikely to exist at low areal densities and would also reach saturation active site densities at Ni^{2+}/H^+ ratios of 0.5 instead of unity. The rate data in Fig. 1 implicate $(Ni\text{-}OH)^+$ as the active structures, with their reactivity being much higher than for the NiO domains that would prevail at Ni^{2+}/H^+ ratios above stoichiometric exchange. Selectivities were not affected by Ni^{2+}/H^+ ratios (Fig. 1), indicating that residual H^+ from Al-MCM-41, present at sub-stoichiometric Ni contents, do not catalyze regioisomerization or oligomerization at the conditions of these experiments.

2,6-di-*tert*-Butylpyridine (DTBP) is a non-coordinating amine that titrates Brønsted-acid sites in solids irreversibly and selectively during isomerization [32] and dehydration [33] reactions, leading to full suppresion of reactivity. Fig. 3 shows ethene dimerization rates (per mass) on Ni-MCM-41 (Ni^{2+}/H^+ = 0.1, 0.8) before (left panel) and during (right panel) DTBP flow (0.5 kPa, 448 K) as a function of the cumulative titrant uptake (per H^+ in Al-MCM-41 sample before Ni exchange). On both samples, rates decreased monotonically with DTBP uptakes and reached undetectable levels at $DTBP/H^+$ ratios near unity, consisting with the involvement of OH^- in $(Ni\text{-}OH)^+$ in dimerization turnovers and with the same number of protons in Ni-Al-MCM-41 and the Al-MCM-41 precursor at both exchange levels (Ni^{2+}/H^+ = 0.1, 0.8).

CO interacts with Ni^+ and Ni^{2+} sites of low coordination [7,21]. Exposing Ni-MCM-41 samples to 1 kPa CO at 263 K led to an infrared band at ~2200 cm^{-1} (Fig. S3, SI), corresponding to Ni^{2+}-(CO) [34]; these bands are not present in the H-form of Al-MCM-41. Fig. 4 shows dimerization rates (1.5 MPa; 243 K) as a ratio to that before contact with CO pulses as a function of the cumulative CO uptakes (introduced CO molecules per Ni atom) on Ni-MCM-41 samples with Ni^{2+}/H^+ ratios of 0.1 and 0.8, chosen here because they do not appear to contain the inactive bulk-like NiO domains prevalent at higher Ni contents and which may also be able to adsorb CO. The rate decrease as a function of cumulative CO per total Ni is similar for Ni-MCM-41 samples, leading to CO uptakes (per Ni atom) that are similar at these two Ni^{2+}/H^+ ratios. The number of CO molecules that must be introduced in order to fully

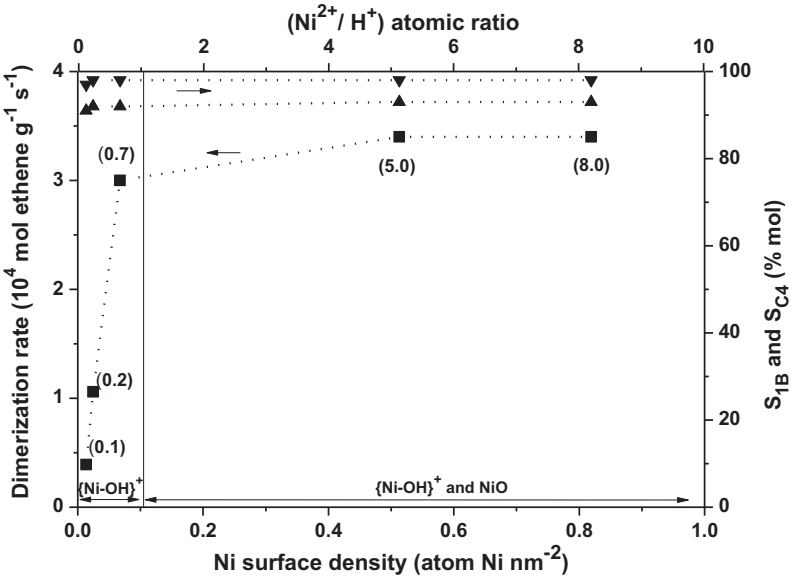

Fig. 1. Ethene dimerization rates (per mass, ■); 1-butene selectivity in C_4 alkenes (S_{1B}, ▲); and C_4 alkenes within products (S_{C4}, ▼) as a function of Ni surface density and Ni^{2+}/H^+ atomic ratio (based on fresh Al-MCM-41: 1.8 · 10^{-4} mol H^+ g^{-1}) (243 K, 1.5 MPa ethene, 4–6% conversion). Ni contents (0.1–8.0% wt.) shown in brackets. Dashed curves denote trends.

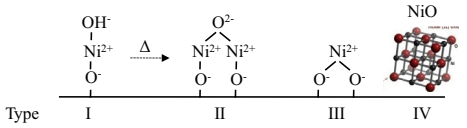

Fig. 2. Ni species on Al-MCM-41 (Si/Al = 40) that could form upon with $Ni(NO_3)_2 \cdot 6H_2O$ solutions, prepared as described in Section 2.1. Ni species are defined as isolated hydroxylated Ni^{2+} monomers (I), Ni^{2+} dimers (II) derived upon thermal treatment (△) of type I species, Ni^{2+} monomers exchanged on two H^+ sites (III), or bulk nickel oxide (IV). Similar species have been shown to form in crystalline aluminosilicates upon contact with Cu^{2+} (aq.) [31].

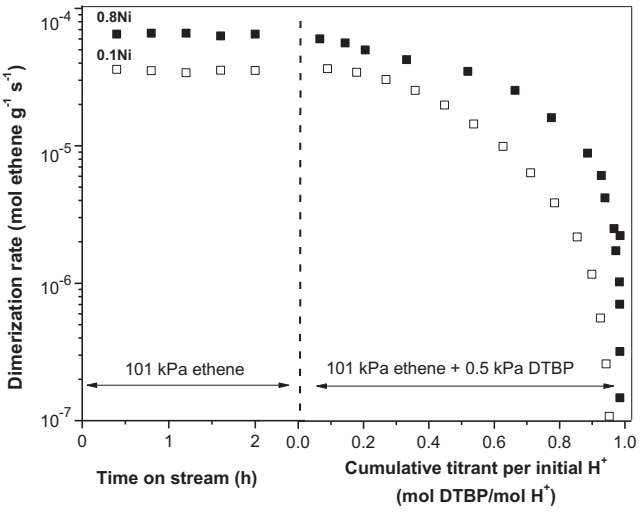

Fig. 3. Ethene dimerization rates at 448 K, 0.1 MPa ethene and an ethene molar rate of 20 mol g^{-1} h^{-1} for 0.1 Ni^{2+}/H^+ (□) and 0.8 Ni^{2+}/H^+ (■) samples on stream (left panel, before titration) and with respect to cumulative titrant per initial H^+ content ($1.8.10^{-4}$ mol H^+ g^{-1}) after addition of 0.5 kPa of 2,6-di-*tert*-butylpyridine (DTBP, right panel). Titration experiments conducted at 448 K on stable dimerization rates and by injecting 0.5 kPa DTBP and 12.5 kPa *n*-hexane at 0.01 mol_{DTBP} g^{-1} h^{-1}. A rate decrease towards a DTBP/H^+ ratio of unity indicates the titration of residual H^+ from Al-MCM-41 and OH^- from $(Ni\text{-}OH)^+$ sites.

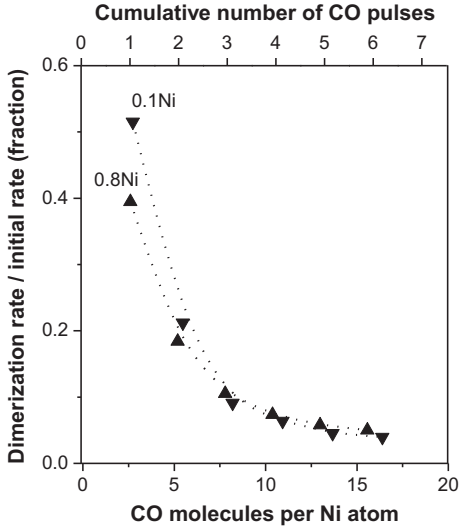

Fig. 4. Ratio of rates after each pulse referenced to the rates measured before CO introduction (per Ni) as a function of introduced CO molecules per Ni atom after each pulse (1% CO/He pulses) for 0.1 Ni^{2+}/H^+ (40 mg, □) and 0.8 Ni^{2+}/H^+ (10 mg, ■) at 243 K, 1.5 MPa ethene and at an ethene molar rate of 20 mol g^{-1} h^{-1}. Each pulse corresponds to 2.5 CO molecules per Ni atom.

suppress dimerization rates exceeds the expected 1:1 CO/Ni^{2+} stoichiometry, because not all molecules in each pulse can access Ni sites by diffusion through intrapore liquids during their passage through the catalyst bed. The fraction of each pulse that is retained by the sample cannot be determined because mass spectrometry cannot distinguish CO and ethene molecules because of their similar mass (28 amu).

The full suppression of rates by both DTBP (Fig. 3) and CO (Fig. 4) implicate the concerted involvement of OH^- and Ni^{2+} centers in dimerization turnovers and the presence of isolated $(Ni\text{-}OH)^+$ species grafted onto the locations set by H^+ in Al-MCM-41. Dimerization turnover rates at 258 K on such species (per Ni) are two orders of magnitude higher than on NiO domains in Al-MCM-41 [21] or isolated Ni^{2+} sites in zeolites [27,28] at around 390 K (Table 1); the poor reactivity of these latter materials appears to reflect their tendency to form Ni^{2+} monomers (type III, Fig. 2), which would require their reduction to Ni^+ in H_2 for the formation of a vicinal proton; leading to inactive Ni^+ and to a proton that is much less active than isolated $(Ni\text{-}OH)^+$ centers.

3.2. Stabilization of active Ni-based sites by the formation of liquid ethene within MCM-41 mesopores

Ethene dimerization rates (r_{ed}) remain constant with time at an ethene pressure of 1.5 MPa and 243 K (Fig. 5). These rates decrease by a factor of 2.5 when ethene pressures are decreased from 1.5 MPa to 0.9 MPa, consistent with rates that are approximately second-order in ethene pressure. Deactivation becomes immediately evident upon this decrease in ethene pressure. The curved nature of the semilogarithmic rate plots in Fig. 5 reflect deactivation rate constants (given by the local slopes of these curves) that decrease with time, as deactivation occurs and ethene conversion, and thus the concentration of oligomerization products, concomitantly decrease. These trends are consistent with site blockage by larger oligomers, which prevail at the higher conversions characteristic of earlier reaction times. The prevalence of these longer chains at higher conversions is also evident from higher C_6/C_4 ratios observed at shorter residence times (Fig. S1). C_6/C_4 product ratios, however, also increase with ethene pressure; yet and surprisingly at first glance, dimerization rates are stable and deactivation becomes undetectable at higher pressures, in seeming contradiction to the expected blockage of active centers by longer alkenes (Fig. 5). The deactivation observed at lower pressures can be fully reversed by thermal treatments at 823 K in either an inert (He) or oxidizing (O_2) environment, indicative of desorption as the restoring mechanism and of species that chemisorb reversibly at high temperatures (but not at those of dimerization catalysis).

First-order deactivation constants (k_d) are used here to define the stability of the active Ni sites in samples from:

$$\frac{r_{ed}(t)}{r_{ed}(t_0)} = \exp[-k_d \cdot (t - t_0)] \quad (1)$$

where r_{ed} (t) and r_{ed} (t_0) represent ethene dimerization rates at each time t and at the initial time t_0. Fig. 6 shows deactivation rate constants (k_d; Eq. (1)) as a function of ethene pressure at 243 and 253 K (more details on rate-time data are included Figs. S4 and S5, SI). The k_d values in Fig. 6 show an abrupt increase as the ethene pressure decreases below 1.2 MPa at 243 K and below 1.8 MPa at 253 K. These k_d values are shown in Fig. 7 (left axis) as a function of ethene (P/P_{sat}), the ratio of the ethene pressure to its saturation vapor pressure (P_{sat}) at each temperature. These threshold pressures are slightly lower than the ethene saturation pressures (P/P_{sat} = 0.6–0.7) at each temperature (1.94 MPa at 243 K; 2.55 MPa at 253 K), indicating that stability may coincide with the condensation of ethene within small MCM-41 cylindrical pores of nearly uniform

Table 1
Ethene dimerization rates (per mass, per Ni-atom), C_4 and 1-butene selectivities.

Catalyst				Ethene dimerization						
Support	Ni (%wt.)	Pressure (MPa)	Temperature (K)	Rate (per mass) ($g_{butene}\ g_{cat}^{-1}\ h^{-1}$)	Rate (per Ni-atom) ($mol_{butene}\ mol_{Ni}^{-1}\ h^{-1}$)	Butenes selectivity (% mol)[l]	1-Butene selectivity in C_4 (% mol)[m]	Mean life $1/k_d$ (h)[n]	$(Al/Ni)_{at}$	Ref.
Ni-α-Diimine[a]	–	5.6	308	–	59,000	–	94[a]	–	100	15
Ni-P,N ligands[b]	–	1.0	303	–	61,000	77	–	–	6	16
MOF[c]	2.7	1.5	294	157	6040	94	86	12	70	12
MOF[d]	10.0	1.5	283	205	10,400	94	95	–	70	13
MOF[e]	1.0	5.0	298	400	41,500	97	91	–	500	14
$NiCl_2$ + DEA-MCM[f]	–	0.5	303	–	498,000	95	–	–	10	36
MCM-41[g]	5.0	2.6	393	10	183	95	–	–[d]	0	21
MCM-41[h]	2.0	3.5	423	68	15,700	58	20	91	0	22
SBA-15[h]	2.6	3.5	423	70	14,200	53	20	265	0	22
FAU[i]	3.7	3.5	388	10	530	53	–	65	0	27
BEA[j]	2.5	2.6	393	1	132	58	–	–[h]	0	28
MCM-41[k]	0.2	3.0	258	43	38,900	98 (97)	92 (91)	630	0	This study
	5.0	3.0	258	135	8700	98 (96)	93 (92)	612	0	

[a] Homogeneous Ni (II)-α-Diimine; batch reactor, toluene solvent; modified methylaluminoxane (MAO) activator. Butenes selectivity corresponding to shown for α olefins.
[b] Nickel complexes containing P,N-Chelating Ligands; complex 16c in reference; batch reactor toluene; in the presence of $AlEtCl_2$.
[c] NU-1000-bpy-$NiCl_2$ (Ni-MOF) with Et_2AlCl; flow reactor.
[d] Ni-(Fe)MIL-101 MOF with Et_2AlCl; iron (III) octahedral trimers linked by 2-aminoterephthalates; batch reactor, *n*-heptane solvent.
[e] Ni-MFU4*l* with MAO; batch reactor, toluene solvent.
[f] Homogeneous and supported co-catalysts with $NiCl_2(PBu_3)_2$; batch reactor, toluene solvent; diethylaluminum chloride as co-catalyst on DEAC-MCM-41.
[g] 5.7%wt Ni/AlM41; flow reactor, no solvent. No deactivation detected over 8 h on stream.
[h] Batch reactor, *n*-heptane solvent. 1-butene and cis/trans 2-butene in equilibrium.
[i] Ni-exchanged Na-FAU zeolite (Si/Al = 3); flow reactor, no solvent, 100% conversion.
[j] Commercial H-BEA (Si/Al = 12); flow reactor, no solvent. No deactivation detected over 8 h on stream.
[k] Ni-exchanged Al/MCM-41 (Si/Al = 40); flow reactor, no solvent at 5% (or 40%)conversion.
[l] Butenes (% mol)among products.
[m] 1-butene (% mol) among butenes.
[n] Reciprocal first-order deactivation rate constant (k_d).

(1.0–2.2 nm diameter). The fraction of total pore volume in MCM-41 filled with ethene is shown in Fig. 7 (right axis). N_2-physisorption uptakes (Fig. S6, SI) were used to determine the fraction of mesopores filled with liquid ethene at dimerization conditions. The similar BET surface areas obtained for porous adsorbents using N_2 and ethene as the physisorbed probe molecules [36] and their similar ratios of physisorption to liquid condensation enthalpies (the *c* constant in the BET equation [37]) allows the rigorous use of N_2 uptakes to determine the extent or pore filling by liquid ethene.

Fig. 8 shows the pore diameter of Ni-Al-MCM-41 (Ni^{2+}/H^+ = 5.0) as a function of fraction of pore volume filled with ethene; the inset shows the differential pore volume distribution as a function of the pore diameter, obtained from N_2 uptakes at 77 K (Fig. S6, SI). Such distribution shows that the fraction of the total pore volume that represents complete filling of the ordered mesoporous channels in MCM-41 (1.0–2.2 nm diameter) is 0.62. These values correspond to the relative ethene pressures (P/P_{sat} = 0.6–0.7) that lead to undetectable deactivation in Ni-Al-MCM-41 samples, indicating that the presence of an extended liquid phase in 1.0–2.2 nm pores in contact with the Ni-based active sites leads to their unprecedented stability during ethene dimerization.

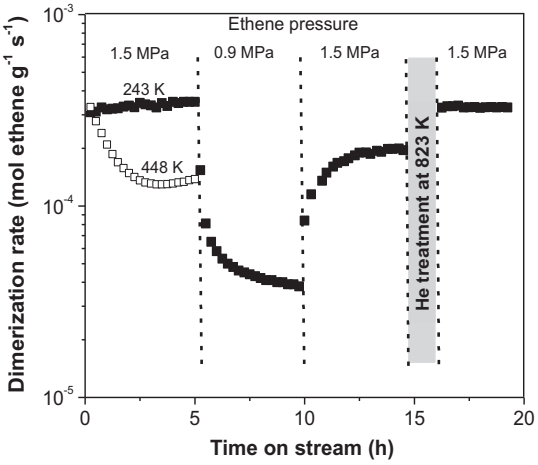

Fig. 5. Ethene dimerization rates (per mass) on the 5.0 Ni^{2+}/H^+ sample vs. time-on-stream at 0.9–1.5 MPa ethene, at an ethene molar rate of 20 mol g^{-1} h^{-1}, at 243 K (■) and 448 K (□), and after treatment in He for 1 h at 823 K (■).

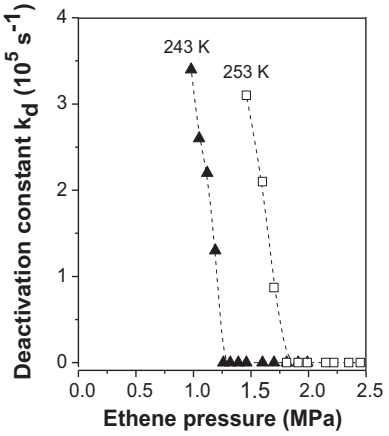

Fig. 6. First-order ethene dimerization deactivation constants (k_d, Eq. (1)) as a function of ethene pressure at 243 K (▲) and 253 K (□) on Ni-Al-MCM-41 (Ni^{2+}/H^+ = 5.0) (20 mol_{C2H4} g^{-1} h^{-1}; k_d from slopes of the semi-logarithmic plots in Figures S4 (243 K) and S5 (253 K)).

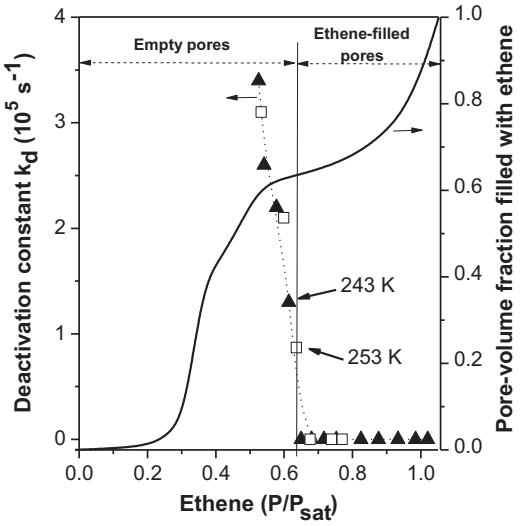

Fig. 7. First-order deactivation constant (k_d, Eq. (1)) on Ni-Al-MCM-41 (Ni^{2+}/H^+ = 5.0) (from Figs. S4 (243 K, ▲) and S5 (253 K, □)) and fraction of pore volume filled with liquid ethene (estimated from N_2 uptakes at 77 K) as a function of the ratio of ethene pressure to its saturation pressure at each temperature. Vertical line corresponds to relative pressure required to fill all MCM-41mesopores smaller than 2.2 nm in diameter.

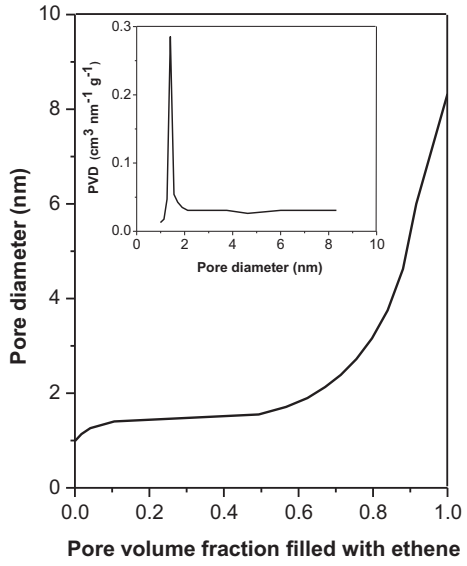

Fig. 8. Pore diameter on Ni-Al-MCM-41 (Ni^{2+}/H^+ = 5.0) as a function of fraction of pore volume filled with ethene. Inset graph depicts the pore volume distribution (PVD) as a function of pore diameter on Ni-Al-MCM-41 (Ni^{2+}/H^+ = 5.0). Pore diameter and pore volume distribution data obtained from the N_2-physisorption uptake from Figure S6 at 77 K and 0.1 MPa. Here, ethene is used in place of N_2, and N_2-physisorption data at 77 K are extrapolated to the studied temperatures (243–253 K) that allow ethene condensation in Ni-MCM-41 pores.

3.3. Kinetic and mechanistic analysis of ethene dimerization pathways

Fig. 9 shows the values of second-order dimerization rate constants (α) as a function of ethene pressure (P_E). Ethene dimerization rates (r_{ed}) are second-order in ethene pressure at 448 K and can be described with a constant value of α:

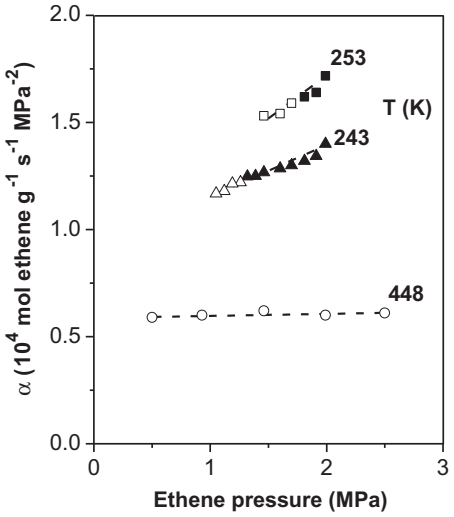

Fig. 9. Second-order ethene dimerization rate constants (α), after correction with ethene pressure, as a function of ethene pressure on Ni-Al-MCM-41 (Ni^{2+}/H^+ = 5.0) at an ethene molar rate of 20 mol g^{-1} h^{-1}. Filled symbols at 243 K (▲) and 253 K (■) represent ethene liquid-filled pores and empty symbols at 243 K (△), 253 K (□) and 448 (○) denote conditions where pores ≤ 2.2 nm are empty (as inferred from N_2 pore filling models in Figure S6). Dimerization rate data obtained from immediate rate changes (as required to evaluate kinetic responses) after change in ethene pressure. Dashed lines used as trends.

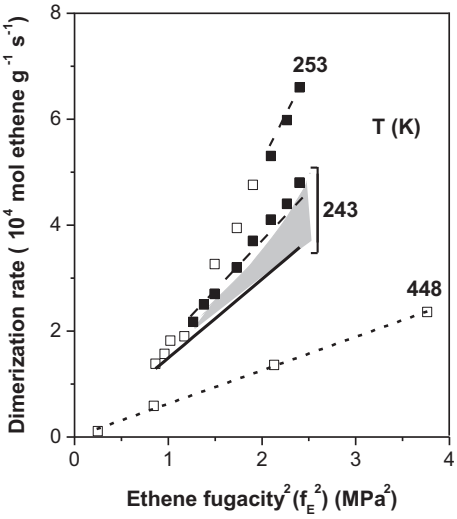

Fig. 10. Dimerization rates (symbols), trends for ideal thermodynamics ($\gamma^{\ddagger} = \varphi_E = 1$; 243 K; solid line) and rates predicted by Eq. (1) (dashed lines) as a function of the square of ethene fugacity on Ni-Al-MCM-41 (Ni^{2+}/H^+ = 5.0). Dimerization rate data at 243 and 253 K obtained from immediate rate changes (as required to evaluate kinetic responses) after change in ethene pressure in Figs. S4 and S5, respectively. Rates at 448 K measured after 5 h (Fig. 5). Ideal rates from slope of rates at 0.8 MPa^2 at 243 K. Symbols (□) and (■) denote conditions leading to intrapore gas and liquid, respectively.

$$r_{ed} = \alpha \cdot P_E^2 \qquad (448\ K) \tag{2}$$

At subambient temperatures, however, α values increase with ethene pressure (Fig. 9) as conditions approach the condensation point of ethene molecules. At such conditions, the ethene gas phase can no longer be considered to behave as a thermodynamically ideal system, and any treatment of chemical dynamics must rely on transition state formalisms that rigorously account for such non-idealities and for the preeminence of chemical potentials and fugacities as the relevant kinetic driving forces for chemical reactions.

The effects of ethene pressures (or fugacities) on dimerization rates are consistent with the kinetic relevance of step 1.2 (Scheme 1; k_E), which forms a C—C bond between a gaseous and a bound ethene present at low coverages on Ni centers (Step 1.1, K_E).

Transition state (TS) theory formalisms would then describe dimerization rates (r_{ed}, per unit volume) in terms of the number of transition-state complexes ($C^{\ddagger}$) that convert to products in the time scale of a molecular vibration of frequency ν_b corresponding to the mode that causes the bond to form or cleave (in this case the symmetric vibration of the C—C bond being formed) [38]:

$$r_{ed} = \nu_b \cdot C^{\ddagger} \tag{3}$$

These TS treatments are based on thermodynamic constructs that naturally incorporate thermodynamic non-idealities in terms of the chemical potential and fugacity (f_E) of ethene [32,33]. The relevant concentration of transition state structures require, in turn, their activity coefficient ($\gamma^{\ddagger}$) within intrapore liquids. Dimerization rates (r_{ed}) under non-ideal solutions [38–40]:

$$r_{ed} = \left(\frac{k_B T}{h}\right) \cdot e^{-\Delta G^{\ddagger}/RT} \cdot \frac{f_E^2}{\gamma^{\ddagger}} \tag{4}$$

where k_B is the Boltzmann constant; h, the Planck constant, and f_E is proportional to P_E through a fugacity coefficient (φ_E). $\Delta G^{\ddagger}$ is the Gibbs free energy difference between the C—C bond formation TS ($G^{\ddagger}$) in step 1.2 in its thermodynamically ideal state and two ethene molecules as an ideal ($2G_{E(g)}$):

$$\Delta G^{\ddagger} = G^{\ddagger} - 2G_{E(g)} \tag{5}$$

The corrections to the ethene pressure values dictated by the non-ideal character of the extrapore gas phase (e.g., φ_E = 0.80 at 243 K, 1.99 MPa; from Eq. (S1), Section S8 [41]) give f_E values that describe rates ($r_{ed} \sim f_E^2$, Fig. 10) with a slightly stronger effect of fugacity than prescribed by Eq. (4) when the TS structures bound at Ni sites are considered to be ideal (i.e. $\gamma^{\ddagger} = 1$) (solid line, Fig. 10) at 243 K. These rate enhancements reflect the solvation of the dimerization TS by the intrapore liquids ($\gamma^{\ddagger} < 1$), which render such structures also different from those in contact with an ideal gas phase. The non-ideal character of this TS was treated by estimating the activity coefficients for dilute 1-butene in liquid ethene (γ_{1B}), used as a proxy for the bimolecular TS ($\gamma^{\ddagger}$) (UNIFAC model with group contributions [42]; Section S9, Table S1), as a function of ethene pressure. Such estimates give a $\gamma^{\ddagger}$ value of 0.80 at 243 K, with negligible effects of ethene pressure in the pressure range required to form intrapore liquids in MCM-41. These $\gamma^{\ddagger}$ values account for the deviations from ideal systems as channels are filled by a denser liquid phase. They accurately capture the rate enhancements observed relative to the ideal systems ($\gamma^{\ddagger} = 1$), as prescribed by Eq. (4) (dashed curve; Fig. 10) and indicative of the stabilization of the dimerization TS relative to its ideal state by the intrapore liquids. The rate enhancements at 253 K are also well described by Eq. (4) ($\gamma^{\ddagger}$ = 0.79) (Fig. 10), while conditions that do not lead to intrapore liquids and to ideal gas behavior by ethene

$$C_2H_4(g) + * \rightleftharpoons C_2H_4* \qquad (K_E; 1.1)$$

$$C_2H_4(g) + C_2H_4* \rightleftharpoons (C_2H_4 - C_2H_4)^{\ddagger} \longrightarrow C_4H_8 + * \qquad (k_E; 1.2)$$

Scheme 1. Ethene dimerization elementary steps (*; a Ni active center).

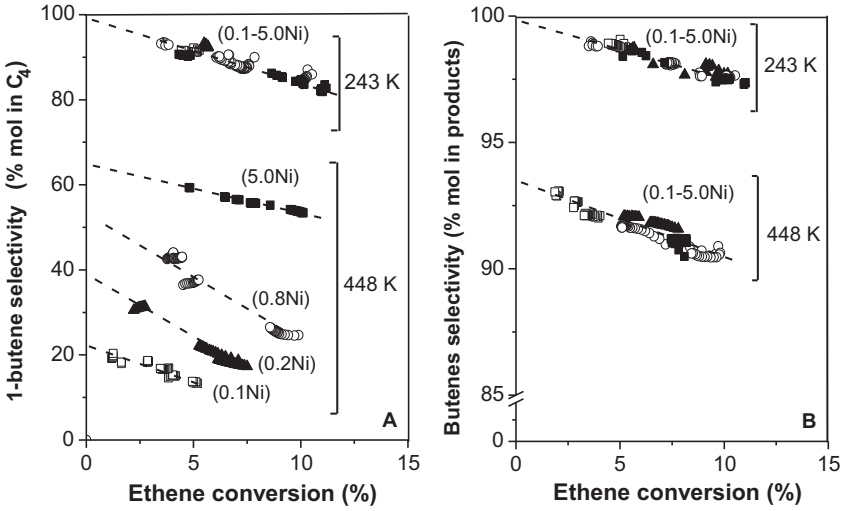

Fig. 11. 1-Butene (Fig. 11a) and butenes selectivity (Fig. 11b) as a function of ethene conversion (ethene molar rate of 10–20 molg^{-1} h^{-1}) at 1.5 MPa ethene and 243 K (after 5 h on stream) and 448 K (after 5 h on stream) for Ni^{2+}/H^+ ratios (in brackets) of 0.1 (□), 0.2 (▲), 0.8 (○) and 5.0 (■). Dashed lines used as trend.

(e.g. 448 K, and open symbols at 243–253 K; Fig. 10) can be described, as expected, by $\gamma^{\ddagger}$ and φ_E values of unity. The slight increase in rates with temperature (243 K to 253 K) at conditions that prevent deactivation reflect the small values of dimerization activation barrier; while the lower rate observed at higher temperatures (448 K, Fig. 10) is a consequence of very rapid initial deactivation at the momentary high conversion conditions expected at such higher temperatures and the concomitant loss of a significant fraction of the Ni active sites (Fig. 5).

3.4. Mechanistic interpretations of primary and secondary reactions during Ni-catalyzed ethene dimerization

The sole formation of 1-butene at very short residence times and low ethene conversions (243 K; Fig. 11a) reflects its direct formation as the sole primary dimerization product, defined here as that formed after a single surface sojourn and without intervening desorption and readsorption events. The selectivity to other regioisomers increases as conversion increases, but these selectivity values and trends are identical for catalysts with a broad Ni content (Ni^{2+}/H^+ = 0.1–5.0); such data indicate that Ni sites, instead of residual protons from Al-MCM-41, account for any secondary isomerization events of primary 1-butene products at these low temperatures (243 K, Fig. 11a). Similar trends with conversion are evident at 448 K (after 5 h on stream), but 1-butene selectivities are much lower than those at 243 K for all ethene conversions. These temperature effects predominantly reflect the lower values of primary 1-butene selectivities (evident by extrapolation to zero ethene conversion; Fig. 11a), which decrease as the Ni content decreases, apparently as a result of the isomerization reactivity of residual protons; such secondary reaction rates become comparable to those of ethene dimerization as the H^+/Ni^{2+} ratio increases with decreasing Ni content. In fact, C_4 regioisomers reach equilibrium compositions on the sample with the largest number of protons (H^+/Ni^{2+}=10), even at <5% conversion (K_{eq} = 5.4 for *trans*-2-butene/1-butene; K_{eq} = 2.9 for *cis*-2-butene/1-butene; at 448 K). These high regioisomer selectivities even at very short residence times and low conversions at 448 K give the impression that residual H^+ sites from Al-MCM-41 can form isomers of the 1-butene molecules that form on $(Ni\text{-}OH)^+$ sites. These high regioisomer selectivities reflect instead the very fast nature of double-bond isomerization events on residual H^+ sites at these higher temperatures [11,43], which cause these rearrangements to occur as 1-butene isomers egress via diffusion from a given catalyst aggregate and before they enter the flowing fluid phase in the reactor.

The nearly exclusive formation of C_4 molecules at 243 K and short residence times (Fig. 11b) indicates that only one C—C bond forms during each reactive sojourn at Ni sites and that desorption can occur before subsequent reactions of bound 1-butene species

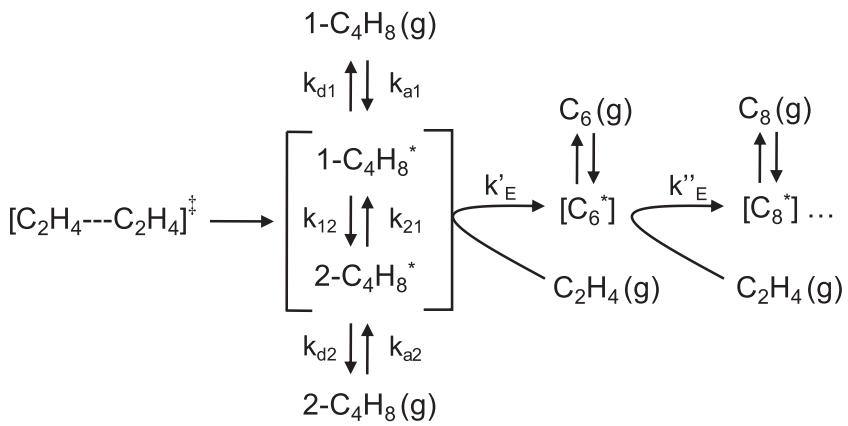

Scheme 2. Alkene oligomerization (k'_E and k''_E) and isomerization (k_{12} and k_{21}) reactions on Ni-MCM-41.

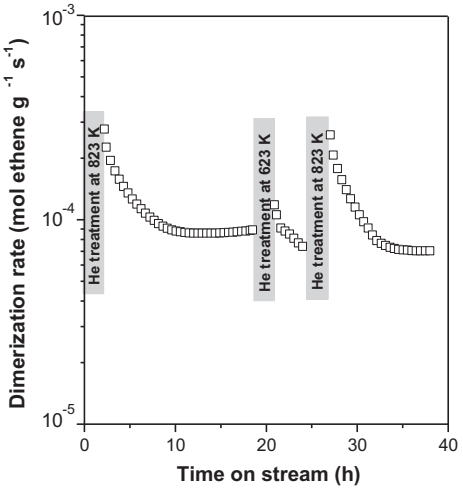

Fig. 12. Time on stream ethene dimerization rates at 448 K, 1.5 MPa ethene, and at an ethene molar rate of 20 mol g^{-1} h^{-1} on Ni-MCM-41 (Ni^{2+}/H^+ = 5.0). He treatments were carried out at 623 and 823 K in flowing He at 0.4 cm^3 g^{-1} s^{-1} by increasing the temperature from 448 K to 623 or 823 K at 0.083 K s^{-1} and holding for 1 h.

with another ethene molecule. Larger chains (C_{4+}) form only via readsorption onto $(Ni\text{-}OH)^+$ sites (instead of H^+ sites) at these temperatures, as shown by the identical C_4 selectivities obtained at all Ni^{2+}/H^+ ratios, including those with sub-stoichiometric Ni contents and a significant number of residual H^+ sites on the Al-MCM-41 support. These trends with conversion and Ni content are also evident at 448 K (Fig. 11b) and at 243 K (Fig. S12) in the absence of intrapore liquids, but the primary C_4 selectivities are 93% and 98%, respectively (instead of 100% on all catalysts at 243 K with intrapore liquids) (Fig. 11b), indicating that more than one C—C bond can form before butenes desorb from Ni sites and that the extended intrapore liquid phase favors the desorption of bound primary butene isomers over their subsequent regioisomerization and oligomerization, thus leading to higher selectivities to primary 1-butene products.

In the reaction sequence depicted in Scheme 1, 1-butenes can desorb from Ni sites (Scheme 1, step 1.2) (k_{d1}, k_{d2}; $\langle k_d \rangle$ is the lumped desorption constants for all butene regioisomers) but can also isomerize or grow, either before desorption or after readsorption, to form bound regiosomers of C_4 alkenes ((k_{12}, k_{21}) or C_6 alkenes (k'_E; C_6^*), which can also desorb, isomerize, or grow. The primary selectivities to 1-butene and C_4 chains depend on the ratios of (k_{d1}/k_{12}) and ($\langle k_d \rangle / k'_E P_E$), respectively. Both kinetic ratios increase as pores fill with liquid ethene (Fig. 11), apparently because of the preferential solvation of the late product-like TS structures that mediate endothermic processes, such as desorption events. Such late transition states reside more fully within, and therefore are more effectively solvated by, the intrapore liquids than the more tightly bound and earlier transition states that mediate the isomerization and growth of bound 1-butene chains formed in primary dimerization events. The readsorption of alkenes, mediated by the same TS as that for their desorption, is similarly favored by intrapore liquids, leading to residence time effects on selectivities that do not depend on temperature or on density of the intrapore fluids (Fig. 11).

3.5. Regeneration of deactivated Ni-Al-MCM-41 catalysts by thermal treatments

Fig. 12 shows the effects of thermal treatments in inert He (623 K, 823 K) on the recovery of dimerization rates of deactivated Ni-MCM-41 (Ni^{2+}/H^+ = 5.0; 448 K, 1.5 MPa ethene). Deactivation events that occur rapidly in the absence of intrapore liquids (0.9 MPa ethene at 243 K, Fig. 5; 1.5 MPa ethene at 448 K, Fig. 12) can be fully reversed by treating samples in He at 823 K. The slightly lower rates (relative to initial rates) observed after treatment in He at 823 K (Fig. 12) reflect the formation of some refractory dehydrogenated species at 448 K, which in contrast, with other blocked sites, cannot be recovered by desorption. The ability to reverse the deactivation by a thermal treatment in an inert environment indicates that Ni sites can be unblocked by the mere desorption of species, instead of only via chemical reduction or oxidation, but that such desorption events require temperatures well above those of dimerization catalysis. Such thermal treatments, whether in inert or chemical environments, would cause irreversible degradation of the structure and catalytic reactivity of organometallic or Ni-MOF catalysts [12–14].

4. Conclusions

This work reports the synthesis and reactive properties of stable and selective ethene dimerization catalysts consisting of Ni active sites dispersed within ordered Al-MCM-41 mesopores, as well as their robustness during thermal regeneration treatments. These catalysts convert ethene to 1-butene with very high selectivity (98% butenes in products; 93% 1-butene in butenes) and turnover rates (>10 s^{-1}; per Ni atom) even at subambient temperatures (243–258 K); they do not exhibit detectable deactivation at these conditions or require aluminoxane activators, essential for homogeneous and Ni-MOF catalysts. Such unique reactivity, selectivity and stability are conferred by an extended ethene liquid phase within MCM-41 channels. We suggest that such liquids preferentially solvate the transition states that mediate desorption of adsorbed products, thus preventing their isomerization and growth, and the formation of stranded oligomers that block Ni sites. Such stability allows to identify kinetically relevant isolated Ni sites, exchanged at H^+ sites on Al-MCM-41 pores.

The application of Ni-based catalysts for oligomerization seems feasible at ambient temperature and pressures leading to alkene condensation. This work provides one of the most novel demonstrations of the role of intrapore liquids in altering reaction pathways through the selective stabilization of specific transition states, and aims to expand this concept to other reactions studying the consequences of intrapore solvation on reactivity and active-site stability.

Acknowledgments

The authors acknowledge a Marie Sklodowska Curie Individual Fellowship (COUPCAT project, H2020 Program) and the Vermeulen Chair endowment for the financial support used to carry out the research. We are also grateful to Dr. Prashant Deshlahra and to Gina Noh for the valuable technical support in the experimental set-up and for helpful discussions. This work was also supported in part by the U.S. Department of Energy, Office of Science, Office of Basic Energy Sciences, under contract number DE-AC05-76RL0-1830.

Appendix A. Supplementary material

Supplementary data associated with this article can be found, in the online version, at http://dx.doi.org/10.1016/j.jcat.2017.06.025.

References

[1] J. Skupinska, Chem. Rev. 91 (1991) 613–648.
[2] D.S. McGuiness, Chem. Rev. 111 (2011) 2321–2341.

[3] R. Robinson Jr., D.S. McGuinness, B.F. Yates, ACS Catal. 3 (2013) 3006–3015.
[4] J.A. Suttil, D. McGuinness, Organometallics 31 (2012) 7004–7010.
[5] R.Y. Brogaard, U. Olsbye, ACS Catal. 6 (2016) 1205–1214.
[6] A.A. Davydov, M. Kantcheva, M.L. Chepotko, Catal. Lett. 83 (2002) 97–108.
[7] M. Lallemand, A. Finiels, F. Fajula, V. Hulea, J. Phys. Chem. C 113 (2009) 20360–20364.
[8] V. Hulea, F. Fajula, J. Catal. 225 (2004) 213–222.
[9] A. Finiels, F. Fajula, V. Hulea, Catal Sci. Technol. 4 (2014) 2412–2426.
[10] M.L. Sarazen, E. Doskocil, E. Iglesia, J. Catal. 344 (2016) 553–569.
[11] M.L. Sarazen, E. Iglesia, ACS Catal. 6 (2016) 7059–7070.
[12] S.T. Madrahimov, J.R. Gallagher, G. Zhang, Z. Meinhart, S.J. Garibay, M. Delferro, J.T. Miller, O.K. Farha, J.T. Hupp, S.T. Nguyen, ACS Catal. 5 (2015) 6713–6718.
[13] J. Canivet, S. Aguado, Y. Schuurman, D. Farrusseng, J. Am. Chem. Soc. 135 (2013) 4195–4198.
[14] E.D. Metzger, C.K. Brozek, R.J. Comito, M. Dincă, ACS Central Sci. 2 (2016) 148–153.
[15] C.M. Killian, L.K. Johnson, M. Brookhart, Organometallics 16 (1997) 2005–2007.
[16] F. Speiser, P. Braunstein, L. Saussine, Acc. Chem. Res. 38 (2005) 784–793.
[17] J.R. Sohn, D.C. Shin, H.W. Kim, J. Ind. Eng. Chem. 13 (2007) 47–56.
[18] J.R. Sohn, Catal. Surv Asia 8 (2004) 249–263.
[19] Y. Pae, S. Lee, J.R. Sohn, Catal. Lett. 99 (2005) 241–248.
[20] A.V. Lavrenov, E.A. Buluchevskii, M.A. Moiseenko, V.A. Drozdov, A.B. Arbuzov, T.I. Gulyaeva, V.A. Likholobov, V.K. Duplyakin, Kinet. Catal. 51 (2010) 404–409.
[21] S. Moussa, M.A. Arribas, P. Concepción, A. Martínez, Catal. Today 277 (2016) 78–88.
[22] R.D. Andrei, M.I. Popa, F. Fajula, V. Hulea, J. Catal. 323 (2015) 76–84.
[23] M. Lallemand, A. Finiels, F. Fajula, V. Hulea, Stud. Surf. Sci. Catal. 170 (2007) 1863–1868.
[24] M. Lallemand, A. Finiels, F. Fajula, V. Hulea, Chem. Eng. J. 172 (2011) 1078–1082.
[25] S. Lin, L. Shi, H. Zhang, N. Zhang, X. Yi, A. Zheng, X. Li, Micropor. Mesopor. Mater. 184 (2014) 151–161.
[26] A. Lacarriere, J. Robin, D. Swierczynski, A. Finiels, F. Fajula, F. Luck, V. Hulea, ChemSusChem 5 (2012) 1787–1792.
[27] J. Heveling, A. Van Der Beek, M. De Pender, Appl. Catal. 42 (1988) 325–336.
[28] A. Martinez, M.A. Arribas, P. Concepcion, S. Moussa, Appl. Catal. A 467 (2013) 509–518.
[29] M. Lallemand, O.A. Rusu, E. Dumitriu, A. Finiels, F. Fajula, V. Hulea, Appl. Catal. A 338 (2008) 37–43.
[30] F.T.T. Ng, D.C. Creaser, Stud. Surf. Sci. Catal. 73 (1992) 123–131.
[31] P. Da Costa, B. Moden, G.D. Meitzner, D.K. Leez, E. Iglesia, Phys. Chem. Chem. Phys. 4 (2002) 4590–4601.
[32] W. Knaeble, R.T. Carr, E. Iglesia, J. Catal. 319 (2014) 283–296.
[33] C.D. Baertsch, K.T. Komala, Y.H. Chua, E. Iglesia, J. Catal. 205 (2002) 44–57.
[34] K. Góra-Marek, A. Glanowska, J. Datka, Microp. Mesop. Mater. 158 (2012) 162–169.
[36] J.F. Duncan, Transac. Farad. Soc. 45 (1949) 879–891.
[37] S. Brunauer, S. Emmett, P.H. Teller, J. Amer. Chem. Soc. 60 (1938) 309–319.
[38] R.J. Madon, E. Iglesia, J. Mol. Catal. A Chem. 163 (2000) 189–204.
[39] J.B. Butt, Reaction Kinetics and Reactor Design, second ed., Marcel Dekker, 2000, pp. 113–150.
[40] M. Boudart, Kinetics of Chemical Processes, Prentice-Hall, 1968, pp. 33–55.
[41] D.Y. Peng, D.B. Robinson, Ind. Eng. Chem. Fundam. 15 (1976) 59–64.
[42] A. Fredenslund, R.L. Jones, J.M. Prausnitz, AIChE J. 21 (1975) 1086–1099.
[43] L.A. Perea, T. Wolff, P. Veit, L. Hilfert, F.T. Edelmann, C. Hamel, A. Seidel-Morgenstern, J. Catal. 305 (2013) 154–168.